Research Square

Preprints are preliminary reports that have not undergone peer review.
They should not be considered conclusive, used to inform clinical practice,
or referenced by the media as validated information.

Decoupling the Pressure-Induced performance Gains in PEMFC stacks: Dominance of Charge-Transfer Resistance over a 10-200kPa Range

Kefeng Hu
Tongji University
Pingwen Ming
pwming@tongji.edu.cn

of Tongji University
Daijun Yang
Tongji University
Tiankuo Chu
Tongji University
Weibo Zheng
Tongji University
Bing Li
Tongji University

Research Article

Keywords: PEMFCs, gas inlet pressure, performance, resistance

Posted Date: November 11th, 2026

DOI: https://doi.org/10.21203/rs.3.rs-11517085/v1

License: This work is licensed under a Creative Commons Attribution 4.0 International License.
Read Full License

Additional Declarations: No competing interests reported.

Abstract

Appropriate operating conditions are considered one of the key factors for ensuring long-term stability, long lifetime, and high efficiency of proton exchange membrane fuel cells(PEMFCs). In this study, the influence of gas inlet pressure on the performance, high-frequency resistance (HFR), impedance, and flow resistance of a PEMFC stack is systematically investigated over a wide pressure range of 10–200 kPa. The experiments are conducted on an 8-cell stack (containing 3 active cells and 5 dummy cells). The operating conditions are controlled at a current density of 1000 mA/cm², a gas relative humidity of 40%, and a cell temperature of 70°C, while the gas pressure is gradually adjusted, and its effects on various indicators are analyzed. The results indicate that the cell performance is significantly improved by increasing the gas pressure; however, the performance gain is first increased and then diminished. Specifically, the average voltage is increased by 69 mV when the pressure is raised from 30/30 to 100/100 kPa, but only by 12 mV when the pressure is further increased from 100/100 to 200/200 kPa. The performance improvement induced by pressure is attributed to the optimization of reversible voltage, ohmic resistance, charge transfer resistance, and mass transfer resistance, among which the most significant contribution is made by the reduction in charge transfer resistance.

1. Introduction

- Proton exchange membrane fuel cells (PEMFCs), as the primary utilization end of hydrogen energy, are widely used in fields such as automobiles, unmanned aerial vehicles (UAVs), and rail transportation due to their advantages of environmental friendliness, zero carbon emissions, and low-temperature quick start capability[1–3]. Despite significant recent gains in PEMFC performance and durability, commercial adoption remains limited-chiefly due to high hydrogen costs and rising market expectations.
- The key to whether a PEMFC can operate continuously, efficiently, and stably lies not only in the quality and performance of its components but also in appropriate operating conditions[4–7]. The operation of a fuel cell involves the coupling effects of multiple physical factors. Its operating conditions include reactant gas pressure, mass flow rate, temperature, and gas humidity, etc.[8, 9]; the coupling of these conditions ensures that the internal state of the cell remains within a suitable range, thereby guaranteeing its high efficiency, high stability, and high durability[10].
- Gas pressure significantly affects the performance of fuel cells, primarily by influencing activation losses, ohmic losses, and mass transport losses, thereby impacting the cell output voltage [11, 12]. Meanwhile, it has been found by a large number of studies[4, 12, 13] that gas pressure has a positive effect on the water content inside fuel cells. Iranzo[11] et al. investigated the effect of different gas pressures ranging from 1.25 to 2.0 bar (abs) on the liquid water content in the cell at different current densities (0.2 A/cm² and 0.4 A/cm²). They found that at low current densities, increasing the gas pressure enhances both the liquid water content and the cell performance, and the effect of cathode pressure is greater than that of anode pressure. However, at higher current densities, the effect of pressure on water content is relatively small. A simulation study by Lu[12] to reveal the

influence of gas pressure on cell performance, attributing the performance improvement mainly to the enhanced membrane conductivity and the higher open-circuit voltage resulting from high backpressure. However, they suggested that increasing pressure reduces the ability to remove water, leading to flooding when the pressure becomes too high. Moreover, as pressure increases, the diffusion rates of oxygen and water vapor decrease.

- Although many studies have investigated the effect of gas pressure and researchers have relatively well understood the underlying mechanisms, they have covered only a limited pressure range, and the magnitude or proportion of the impact on various performance aspects remains unclear. In this study, we select a wider pressure range of 10–200 kPa (absolute pressure,). An inlet pressure of 10 kPa approaches the natural flow resistance of hydrogen under operating conditions, while 200 kPa represents a relatively high inlet pressure currently used in practice. By simultaneously monitoring cell performance, flow resistance, high-frequency resistance (HFR), and electrochemical impedance spectroscopy (EIS), this study compares how different pressures influence each indicator and to what extent.
- This study aims to identify the dominant impedance component responsible for the diminishing performance gain at elevated pressures and to determine whether there exists an optimal pressure window where the trade-off among reversible voltage, ohmic, charge-transfer, and mass-transport resistances is optimized.

2. Experiment

2.1 Material

- The fuel cell stack used for testing in this study consists of eight cells. However, only the three middle cells are real cells, with a total of five dummy cells added at both ends—three at one end and two at the other. The dummy cells are supplied with water but not with reactant gas, for the purpose of avoiding problems such as lower temperatures and uneven stress in the end sections. The membrane electrode assembly (MEA), with an active area of 375cm2, used in this study (UD2Q, Guangdong Horizon New Energy Technologies Co., Ltd), and the carbon paper is 055 (Toray). A metal-graphite composite bipolar plate (D20.0, Guangdong Horizon New Energy Technologies Co., Ltd)consists of an anode plate stamped from a titanium alloy substrate and a cathode plate molded from a graphite substrate. For the anode flow field, parallel wavy flow channels are adopted, while for the cathode, parallel straight flow channels are used. The anode and cathode plates are bonded together using a sealing adhesive.

2.2 Constant-current experiment under different pressure

- All tests in this experiment were conducted using a G100 test station (Greenlight Innovation Co., Ltd., as shown in Fig. 1a). During EIS measurements, a small-amplitude sinusoidal perturbation

current with an adjustable frequency range is applied at a set current using an external Gamry Reference 3000 electrochemical workstation (as shown in Fig. 1b).

- All tests in this study are stably operated at a current density of 1000mA/cm2. Under each condition, the stack was stabilized for more than 15 minutes, and then the cell parameters (such as voltage, internal resistance, and flow resistance) during the last 10 minutes after stabilization were extracted for analysis. The gas pressure condition was gradually adjusted over a range of 10–200 kPa, while other conditions were kept constant, including the gas stoichiometry ratio of 1.8/2.5, a gas relative humidity (RH) of approximately 40%, a cooling water inlet temperature of 70°C, and a cooling water flow rate of 2.5 NL/min.

Table 1
Test condition

Condition	Unit	Value
Current density	mA/cm2	1000
Coolant temperature	°C	70
Stoich-H_2	-	1.8
Stoich-Air		2.5
RH-An	%	40
RH-Ca	%	40
$Q_{coolant}$	NL/min	2.5

2.3 EIS measurement

- EIS measurements were conducted using an electrochemical workstation (Reference 3000, Gamry). The frequency range for the EIS measurements was 0.1Hz to 1kHz, with a constant disturbance current of 18A (the amplitude is 4.8% of the stack operating current). The measured Nyquist plots were fitted in Zview software using the equivalent circuit model shown in Fig. 1c to evaluate the ohmic impedance (R_o), charge transfer impedance (R_{ct}), and mass transfer impedance (R_{mt}) of the stack under different gas inlet pressure[14].

3. Result and discussion

3.1 Performance

- As shown in Fig. 2, as the gas pressure increases, the performance of each of the three cells in the stack gradually improves. However, when the pressure is below 100 kPa, the performance increases substantially with rising pressure; when the pressure exceeds 100 kPa, the performance increase becomes less pronounced. As presented in Table 2, when the anode/cathode inlet pressures are

increased from 30/30 to 100/100 kPa, the average cell performance of the stack rises from 0.630 V to 0.699 V, an increase of 69 mV. In contrast, when the pressures are further increased from 100/100 kPa to 200/200 kPa, the average performance increases only from 0.699 V to 0.711 V, exhibiting a gain of just 12 mV.

To reflect the voltage fluctuations, the standard deviation (*SD*) of each cell voltage over a stabilization period of 10 minutes was calculated. The calculation method of *SD* is as follows:

$$\mathrm{SD}=\sqrt{\frac{\sum_{\mathrm{i}=1}^{\mathrm{n}}\left(E_{\mathrm{i}}-E_{\mathrm{avg}}\right)^{2}}{\mathrm{n}}}$$

1

Where *SD* is standard deviation, n is the number of voltage data points extracted under each condition during stable operation, E_i is the i-th voltage value, E_{avg} is overall arithmetic mean voltage.

As shown in Fig. 3, it can be found that there is no clear correlation between voltage stability and pressure. At low pressures (10–75 kPa), except for the case where the anode pressure was 10 kPa, which gave a relatively large *SD* value, the *SD* values under other pressures were relatively small. The main reason for this may be that when the anode pressure is low, the water removal capacity is reduced, so the cell voltage tends to fluctuate depending on the status of water discharge.

As is shown inFig 3(a)–(d), the voltage fluctuation of each cell during stable operation of the stack. We can observe that in the low-pressure range (10/30–75/75 kPa), the voltage fluctuation of each cell remains small. However, when the pressure reache, as high as 100/100 kPa or even higher, the fluctuation becomes larger. In Fig. 3(a), the *SD* values at 10/30 kPa and 30/30 kPa are considerably larger than that at 75/75 kPa. This occurs mainly because under these conditions, the cell performance gradually improves from its initial state during operation. Although the overall voltage fluctuation remains small, the *SD* still appears relatively large. When the pressure increases to ≥ 100/100 kPa, both the *SD* values and the voltage fluctuation of each cell clearly increase. This indicates that excessively high gas pressure leads to an increase in the water content inside the stack, and even to the presence of liquid water, which in turn causes the voltage to fluctuate more as the stack discharges liquid water.

3.2 HFR

High-frequency resistance (HFR) reflects the ohmic resistance of the fuel cell stack and is primarily related to the conductivity of the proton exchange membrane. It is closely associated with the internal hydration state of the stack, especially the water content of the proton exchange membrane (PEM). As shown in the Fig. 4, the HFR of the stack first decreases and then increases with increasing gas inlet pressure. When the gas pressure is in the range of 30–125 kPa, the HFR decreases as the pressure increases; it reaches a minimum at 125 kPa. When the pressure continues to rise to 200 kPa, the HFR increases with further pressure increase. The fluctuation of HFR does not exhibit a clear correlation with

the change in pressure. However, it has been found by some studies[4, 11, 13, 15] that the water uptake in the membrane inside the stack can be increased by increasing the gas inlet pressure, and the proton conductivity of the membrane is thereby enhanced; therefore, HFR is expected to decrease with increased pressure. The trend in Fig. 4 is taken to indicate that HFR monitoring may be affected by some other interferences apart from membrane conductivity. This issue is clarified by the further decomposition of the ohmic impedance using EIS in the following text.

3.3 Contribution analysis of reversible voltage and HFR

To further elucidate the mechanism underlying the pressure effect on performance, this study separately evaluates the $E_{IR\text{-}match}$ and the $E_{rev\text{-}match}$. $E_{IR\text{-}match}$ is derived by adding the voltage difference attributable to internal resistance changes to the average voltage (E_{avg}) at 10/30 kPa, thereby indicating the voltage variation caused by internal resistance variation with increasing pressure. Here, the lowest pressure of 10/30 kPa is chosen as the benchmark, which can provide a more intuitive reflection of the changes brought about by the increase in pressure. $E_{rev\text{-}match}$ is derived by adding the reversible voltage change due to pressure to the E_{avg} at 10/30 kPa, directly showing how the reversible voltage varies with pressure. The calculation formulas are presented as follows[16–18]:

$$\mathrm{E_{cell}}=\mathrm{E_{rev}}-\mathrm{V_{act}}-\mathrm{V_{ohm}}-\mathrm{V_{con}}$$

2

$$\mathrm{E_{rev}}=\mathrm{E^{0}}+\frac{\mathrm{RT}}{\mathrm{nF}}\ln\left(\frac{\alpha_{\mathrm{H_2}}\alpha_{\mathrm{O_2}}^{1/2}}{\alpha_{\mathrm{H_2O}}}\right)=\mathrm{E^{0}}+\frac{\mathrm{RT}}{\mathrm{nF}}\ln\left(\mathrm{P_{H_2}P_{O_2}^{1/2}}\right)$$

3

$$\mathrm{E_{rev}}=1.229-0.85\times10^{-3}\times\left(\mathrm{T}-298.15\right)+4.308\times10^{-5}\mathrm{T}\times\left(\ln\mathrm{P_{H_2}}+\frac{1}{2}\ln\mathrm{P_{O_2}}\right)$$

4

$$\mathrm{E_{IR-match}}=\mathrm{E_{10/30}}+\mathrm{I}\left(\mathrm{R_{10/30}}\text{-}\mathrm{R_P}\right)$$

5

$$\mathrm{E_{rev-macth}}=\mathrm{E_{10/30}}+\left(\mathrm{E_{rev-P}}-\mathrm{E_{rev-10/30}}\right)$$

6

$$\Delta E_{avg}=E_{avg-P}-E_{avg-10/30}$$

7

$$\Delta E_{IR} = E_{IR-match} - E_{10/30} = I\left(R_{10/30} - R_P\right)$$

8

$$\Delta E_{rev} = E_{rev-match} - E_{10/30} = E_{rev-P} - E_{rev-10/30}$$

9

Where

R_P is the internal resistance at corresponding pressure, and $R_{10/30}$ is the internal resistance at 10/30kPa. In the calculations, the value measured by HFR is uesd.

$E_{avg\text{-}P}$ is the average voltage at the corresponding pressure, and $E_{avg-10/30}$ is the average voltage at 10/30 kPa.

$E_{rev\text{-}P}$ is the reversible voltage at the corresponding pressure, and $E_{rev-10/30}$ is the reversible voltage at 10/30 kPa.

As shown in Fig. 5a, with the increase in gas inlet pressure, E_{avg} gradually and significantly increases, rising by a total of 120 mV when the pressures increased from 10/30 kPa to 200/200 kPa. Erev-match also increases with increasing pressure, but by a smaller margin, with a total increase of 23 mV from 10/30 kPa to 200/200 kPa. However, E_{IR} first increases and then decreases, reaching a maximum at 125/125 kPa, and at 200/200 kPa it shows an increase of only 10 mV compared to the value at 10/30 kPa. As shown in Fig. 5b, it is evident that the voltage improvements due to reversible voltage and internal resistance differences with increasing pressure are markedly smaller than the improvement in the initial average voltage. For example, when the pressure increases from 10/30 kPa to 200/200 kPa, the increase in reversible voltage is 23 mV, accounting for 19.17% of the increase in average voltage (120 mV); the increase due to reduced internal resistance is 10 mV, accounting for 8.33% of the increase in average voltage. This indicates that, in addition to affecting internal resistance and reversible voltage, the increase in pressure leads to other positive effects that contribute to the rise in average voltage, and the magnitude of these effects is greater than that of the internal resistance and reversible voltage effects.

3.4 Gas differential pressure

As shown in the Fig. 6a, the gas pressure drop between the inlet and outlet of both the anode and cathode gases are presented. It can be observed that the overall gas differential pressure of the cathode gas decreases with increasing gas pressure. Although the anode gas differential pressure at 100/100 kPa shows an increase compared to that at 75/75 kPa, the increase is relatively small, while the other gas differential pressure also generally decrease with increasing pressure. A possible reason for the reduction in differential pressure with increasing pressure is that, under the condition of constant gas

mass flow rate, the volumetric flow rate decreases as pressure increases, leading to a decrease in gas velocity and consequently a reduction in friction between the fluid and the medium they flow through. The figure also shows the standard deviation of gas pressure and differential pressure, which reflects the fluctuations in pressure and differential pressure. However, from the Fig. 6b and c, there is no clear trend correlation between the fluctuations of pressure and differential pressure and the gas pressure. However, above 150/150kPa, the pressure fluctuations at the air outlet increased with increasing gas pressure, which may indicate increased accumulation and discharge of liquid water.

3.5 EIS

To further investigate the effect of pressure on polarization loss of each eletrochemical process, the polarization losses under different pressures were measured separately using electrochemical impedance spectroscopy (EIS) [19]. As is shown in Fig. 7a, the first arc in each Nyquist plot, occurring at frequencies above 100 Hz, is associated with the charge transfer resistance(R_{ct}) during the oxygen reduction reaction(ORR) at the cathode, while the second arc, observed at frequencies below 100 Hz, corresponds to mass transport resistance(R_{mt}). The EIS data were analyzed using an equivalent circuit model, and the results are shown in the Fig. 7b. It can be observed that the ohmic resistance (R_{ohm}) decreases with increasing pressure. The mass transfer resistance (R_{mt}) and charge transfer resistance (R_{ct}) decrease with increasing pressure up to 150/150 kPa, but when the pressure exceeds 150/150 kPa, they increase slightly with further pressure increase. This indicates that increasing the pressure can raise the internal water content of the stack, thereby significantly reducing the ohmic resistance of the stack. However, at excessively high pressure, liquid water accumulation may block the gas transport channels, causing the mass transfer resistance to increase instead after exceeding 150/150 kPa. This shows a certain correspondence with the above-mentioned increase in pressure fluctuations at the air outlet.

Following the previous method, the R_{ohm}, R_{ct}, and R_{mt} obtained from the EIS test in Fig. 7b are used to simplify the calculation of the corresponding voltage differences. The related calculation formulas are given as follows:

$$\Delta E_{R_{o-P}} = I\left(R_{ohm-10/30} - R_{ohm-P}\right)/3$$

10

$$\Delta E_{R_{ct-P}} = I\left(R_{ct-10/30} - R_{ct-P}\right)/3$$

11

$$\Delta E_{R_{mt-P}} = I\left(R_{mt-10/30} - R_{mt-P}\right)/3$$

12

Where

$R_{ohm-10/30}$ is the ohmic resistance at 10/30kPa, and R_{ohm-P} is the ohmic resistance at corresponding pressure

$R_{ct-10/30}$ is the charge transfer resistance at 10/30kPa, and R_{ct-P} is the charge transfer resistance at corresponding pressure

$R_{mt-10/30}$ is the mass transport resistance at 10/30kPa, and R_{mt-P} is the mass transport resistance at corresponding pressure.

ΔE_{Rohm-P}, ΔE_{Rct-P}, and ΔE_{Rmt-P} represent the voltage increases resulting from the reduction in impedance at each gas pressure relative to that at 10/30 kPa.

All the above *R* values are the impedances of the stack, averaged over three real electrodes; similarly the total voltage should be divided by cell number 3.

As shown in Fig. 8, the voltage differences caused by various impedances under different gas pressures are presented. Although the simplified calculation method may not yield precise absolute values for the actual voltage differences, it reliably reflects the trends and relative extents. It can be observed that as the pressure increases, the voltage difference for each impedance first rises and then falls, generally peaking at 150/150 kPa and 175/175 kPa. Among them, the voltage difference due to charge transfer impedance is the largest, followed by mass transfer impedance, and finally ohmic impedance. This indicates that pressure enhancement improves all three types of impedance, with the improvement in charge transfer impedance contributing most significantly to the voltage increase. The performance improvement brought by the improvement of the three impedances is the largest before 100 kPa, and the corresponding improvement from 100 to 200 kPa is smaller, which is consistent with the previous trend of stack performance increasing with pressure. According to the findings of Lu[12] et al., the diffusion rates of oxygen and water vapor decrease as the gas pressure increases, which consequently exacerbates concentration polarization loss and reduces water vapor, thereby leading to flooding. Although we did not observe obvious flooding under high pressure in this study, the variation in ohmic resistance reveals an increase in water content. Therefore, the diminished improvement in charge transfer resistance and mass transfer resistance at pressures above 150 kPa, as reported in this paper, suggests that the internal water content has become sufficiently high to impede gas transport.

4. Conclusion

In this study, the effect of gas pressure on the performance of a proton exchange membrane fuel cell stack was systematically investigated over a wide pressure range. The main findings are as follows:

1. Cell performance is significantly improved by increasing gas pressure, but the incremental gain is diminished as the pressure rises. When anode/cathode inlet gas pressures are increased from 30/30 to 100/100 kPa, an average voltage increase of 69 mV is observed; when it is further increased to 200/200 kPa, only a 12 mV increment is obtained. Because when the pressure is

increased from 10/30 kPa to 100/100 kPa, the improvements in ohmic impedance, charge transfer impedance, and mass transfer impedance result in the largest performance gain, whereas when the pressure is further increased, the performance improvement brought by each impedance decreases significantly.

2. The performance improvement brought by pressure is associated with the improvements in reversible voltage, ohmic resistance, charge transfer resistance, and mass transfer resistance, among which the most significant effect is contributed by the improvement in charge transfer resistance. The degree of its influence is even comparable to the sum of the effects of reversible voltage, ohmic resistance, and mass transfer resistance.
3. The stability of cell voltage is relatively good when the gas pressures are less than 75 kPa, but the voltage fluctuation increases significantly when the inlet pressures exceeds 100 kPa. This is because a higher pressure increases the water content inside the stack, leading to accumulation and discharge of localized liquid water, which in turn causes voltage fluctuations.
4. The ohmic resistance monotonically decreases with increasing pressure. The charge transfer resistance and mass transfer resistance decrease with increasing pressure up to 150/150 kPa, and then increase slightly thereafter. Appropriate pressurization enhances reaction kinetics and mass transfer, but excessive pressurization offers limited further improvement in impedance and may even introduce negative effects.

Declarations

Author Contribution

Hu : writing the main manuscript, conceptualization, methodology, validation, analysis;Yang. Ming. Li: funding acquisition, supervision;Chu. Zheng: supervision, project administration,resources;All authors reviewed the manuscript.

Acknowledgement

This work was supported by the National Key R&D Program of China (No.2023YFB2504205) and the National Natural Science Foundation of China (No.52576226), and the Tongji-Horizon Joint Innovation Lab for Hydrogen Energy & Fuel Cell

References

1. Xiao Y et al (2025) Degradation behavior of ionomer in the cathode catalyst layer of polymer electrolyte fuel cells. Appl Energy, 389
2. Hu K et al (2023) Three-dimensional multiphase simulation of a partially narrowed flow field configuration for a high-performance polymer electrolyte membrane fuel cell. Appl Therm Eng, 223

3. Bunyan ST et al (2023) The Effect of Flow Field Design Parameters on the Performance of PEMFC: A Review. Sustainability, 15(13)
4. Qi P et al (2025) A review of water management in proton exchange membrane fuel cell systems. Sustainable Energy Fuels 9(1):72–97
5. Wei F, Kosakian A, Secanell M (2023) Effect of operating conditions and micro-porous layer on the water transport and accumulation in proton exchange membrane fuel cells. Chem Eng J, 471
6. Sanchez DG et al (2015) Analysis of the Influence of Temperature and Gas Humidity on the Performance Stability of Polymer Electrolyte Membrane Fuel Cells. J Electrochem Soc 163(3):F150–F159
7. Chippar P et al (2014) Effects of inlet relative humidity (RH) on the performance of a high temperature-proton exchange membrane fuel cell (HT-PEMFC). Int J Hydrog Energy 39(6):2767–2775
8. Soomro IA et al (2023) Influence of Operating and Electrochemical Parameters on PEMFC Performance: A Simulation Study. Membr (Basel), 13(3)
9. Kahraman H (2023) Experimental and numerical investigation of the effect of variable operating conditions on PEMFC performance. Therm Sci, 27(4 Part B): p. 3089–3100
10. Huang X et al (2006) Mechanical endurance of polymer electrolyte membrane and PEM fuel cell durability. J Polym Sci Part B: Polym Phys 44(16):2346–2357
11. Iranzo A, Salva JA (2018) Effect of Anode/Cathode Operating Pressures on the Liquid Water Content and Performance of a PEM Fuel Cell. Fuel Cells 18(6):742–747
12. Lu JB et al (2019) Pressure Effect on the PEMFC Performance. Fuel Cells 19(3):211–220
13. Ko D et al (2018) Investigation of the effect of operating pressure on the performance of proton exchange membrane fuel cell: In the aspect of water distribution. Renewable Energy 115:896–907
14. Lu Y et al (2026) Post-mortem analysis of the degradation behavior of the fuel cell gas diffusion layer under near to water boiling point conditions. Chem Eng J, 528
15. Reshetenko TV et al (2011) Systematic study of back pressure and anode stoichiometry effects on spatial PEMFC performance distribution. Electrochim Acta 56(24):8700–8710
16. Arbabi F (2012) Numerical Modeling of an Innovative Bipolar Plate Design Based on the Leaf Venation Patterns for PEM Fuel Cells. Int J Eng, 25(3 (C)).
17. Bankupalli PT et al (2020) Operational Adaptability of PEM Fuel Cell for Optimal Voltage Regulation With Maximum Power Extraction. IEEE Trans Energy Convers 35(1):203–212
18. Baschuk JJ *Modelling of polymer electrolyte membrane fuel cells with variable degrees of water flooding*.
19. Todorovski E et al (2026) Understanding water management and cathode performance in LT-PEMFCs via EIS and DRT diagnostics. Energy Rep, 15

Figures

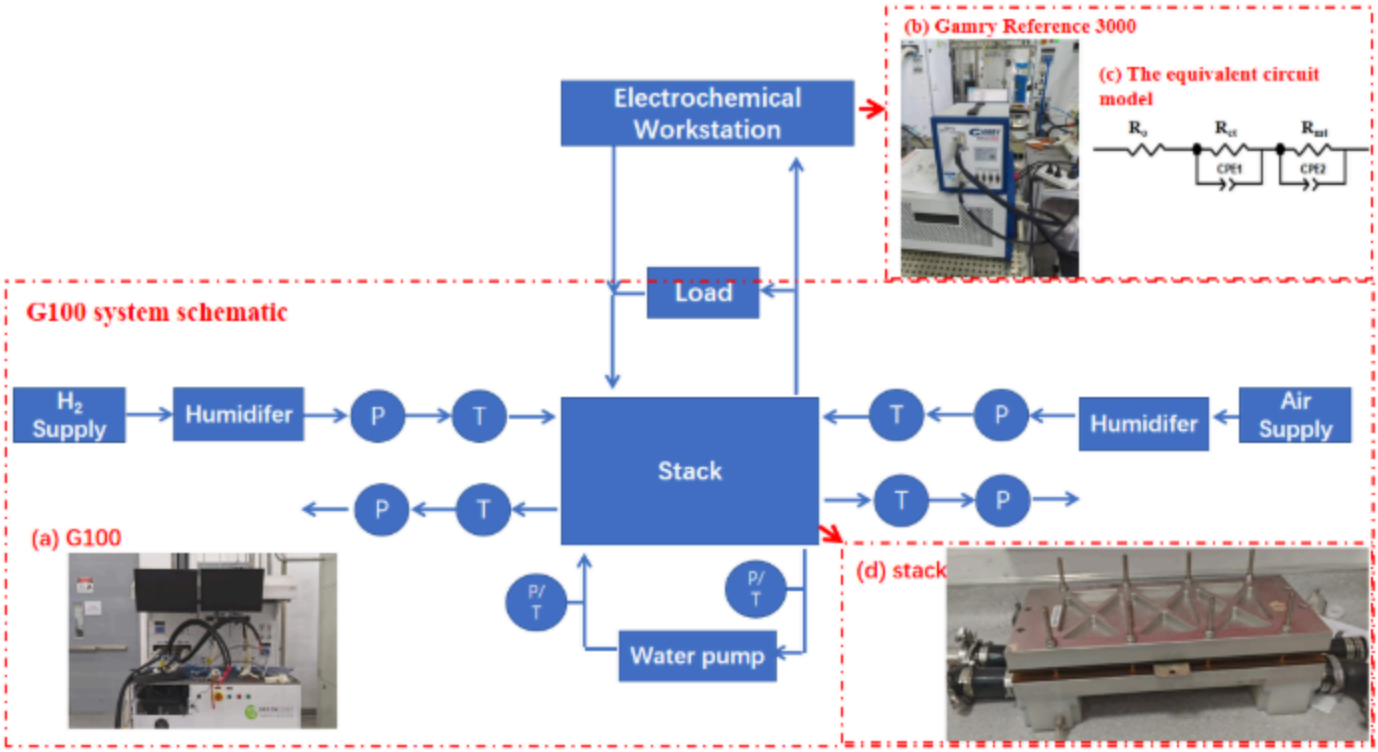


Figure 1

The Schematic diagram of the experimental system:(a) G100 test station; (b) Gamry Reference 3000 electrochemical workstation; (c) the equivalent circuit model; (d) stack

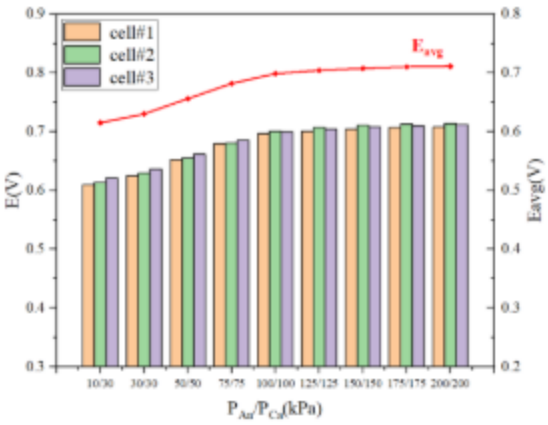


Figure 2

Individual cell voltages and average voltage of the stack under different inlet gas pressures

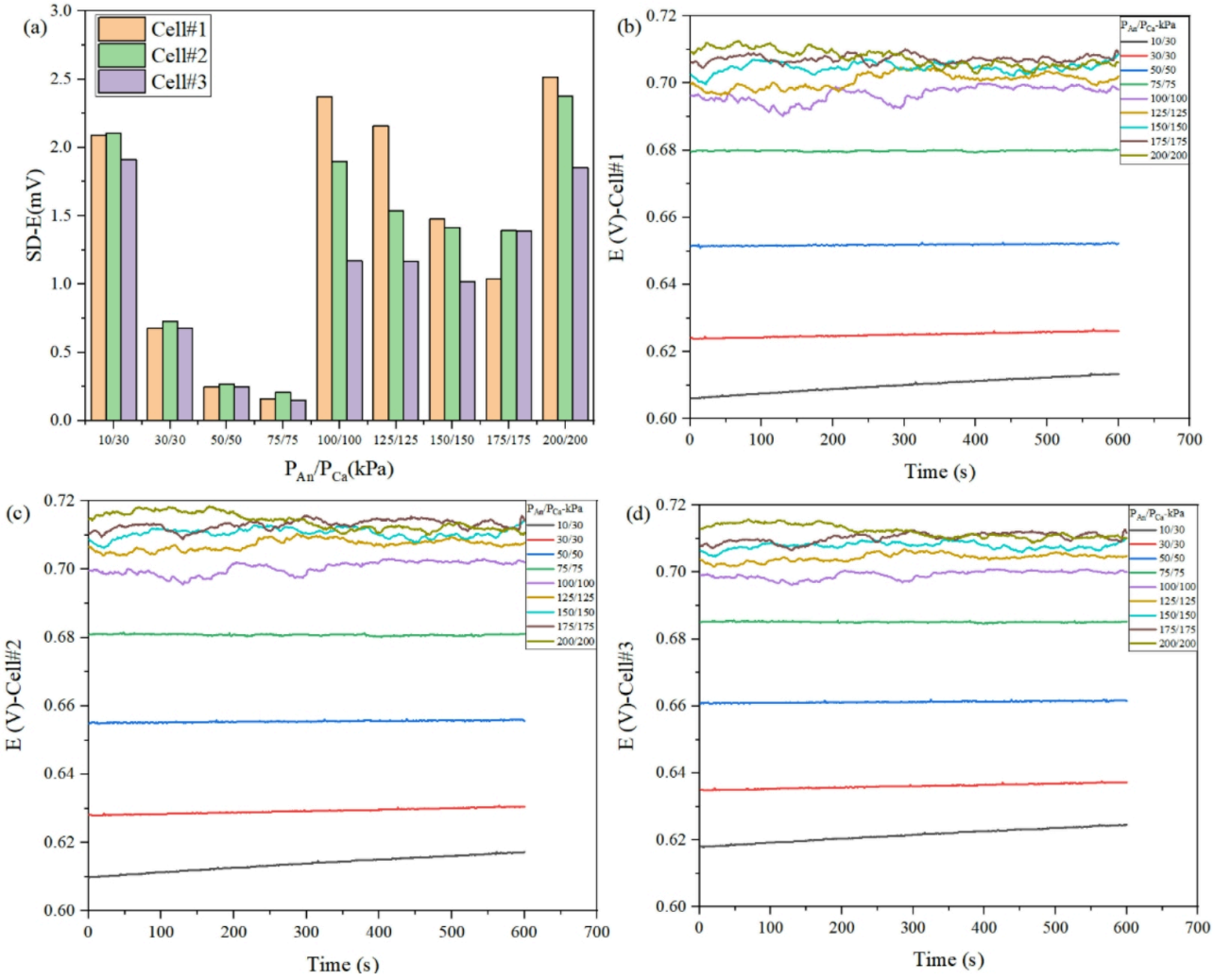


Figure 3

The voltage fluctuation of each cell under different reactant gas pressure: (a) *SD*; (b) Cell#1;(c) Cell#2; (d)Cell#3

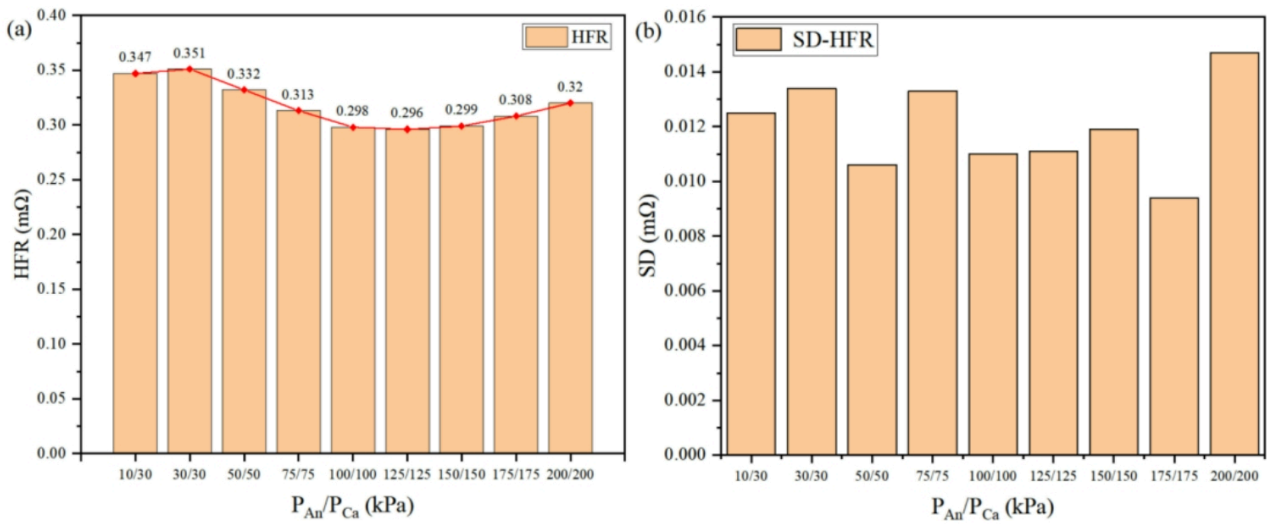


Figure 4

The HFR and its SD under different gas pressure: (a)HFR; (b)SD

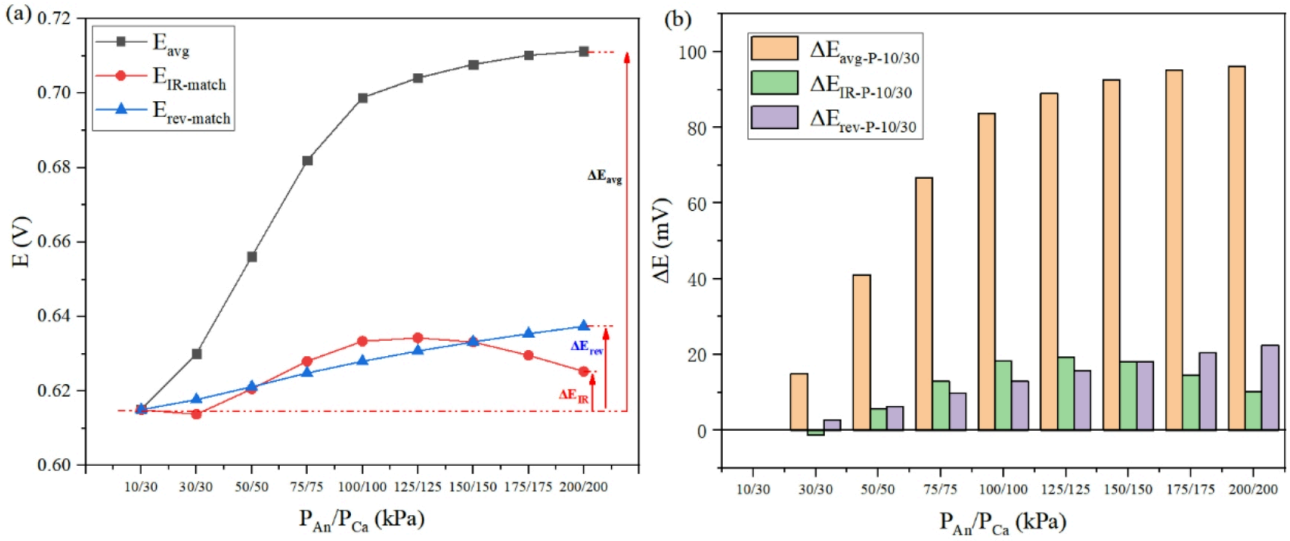


Figure 5

Effect of gas pressure on stack voltage:(a) the original average voltage of the stack(E_{avg}, $E_{IR\text{-}free}$, and $E_{rev\text{-}match}$); (b) the increments relative to the values at 10/30kPa

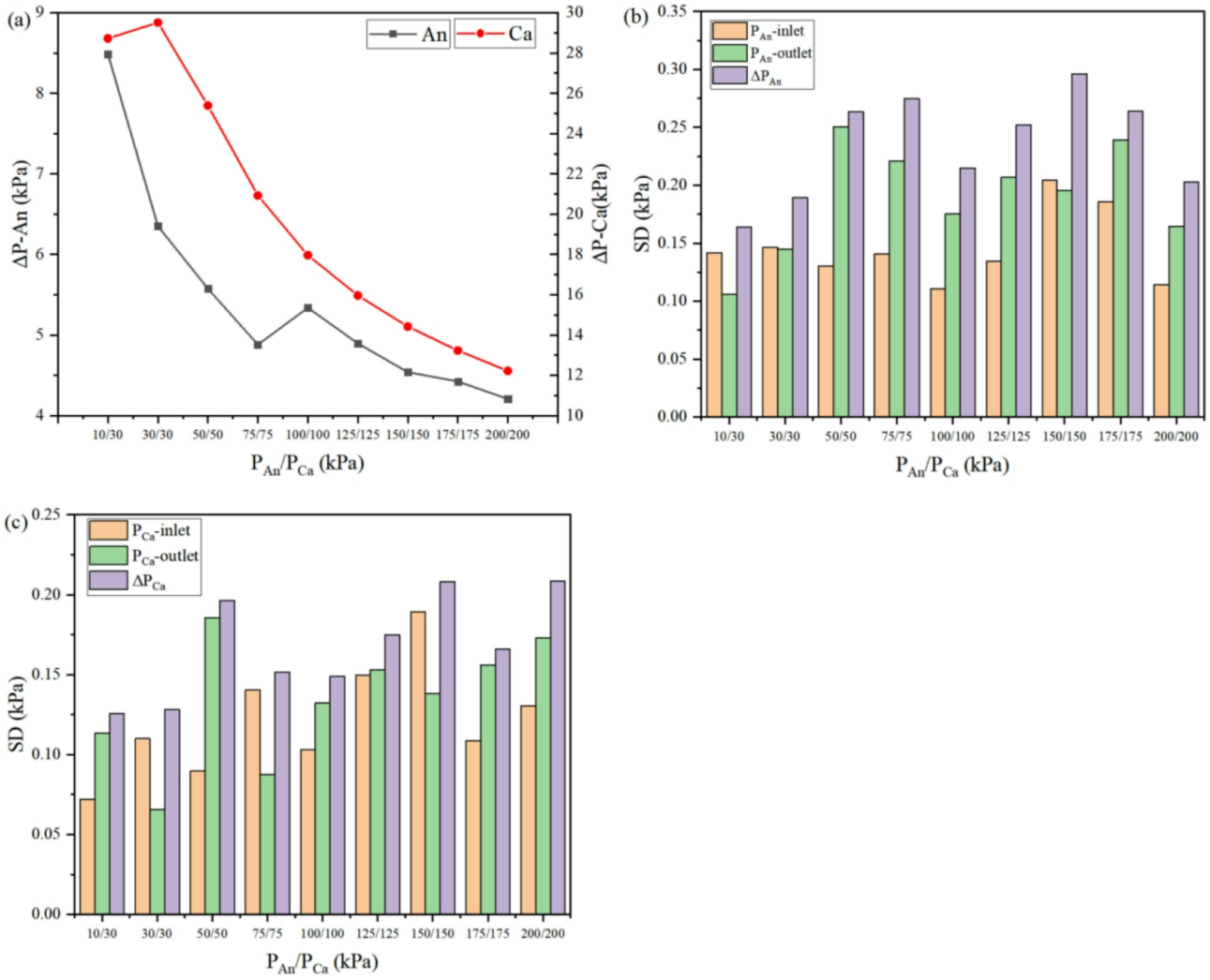


Figure 6

Effects of inlet gas pressure on: (a) gas differential pressure of anode and cathode; (b)the SD of anode gas inlet/outlet pressures and differential pressure; (c) SD of cathode inlet/outlet pressures and differential pressure.

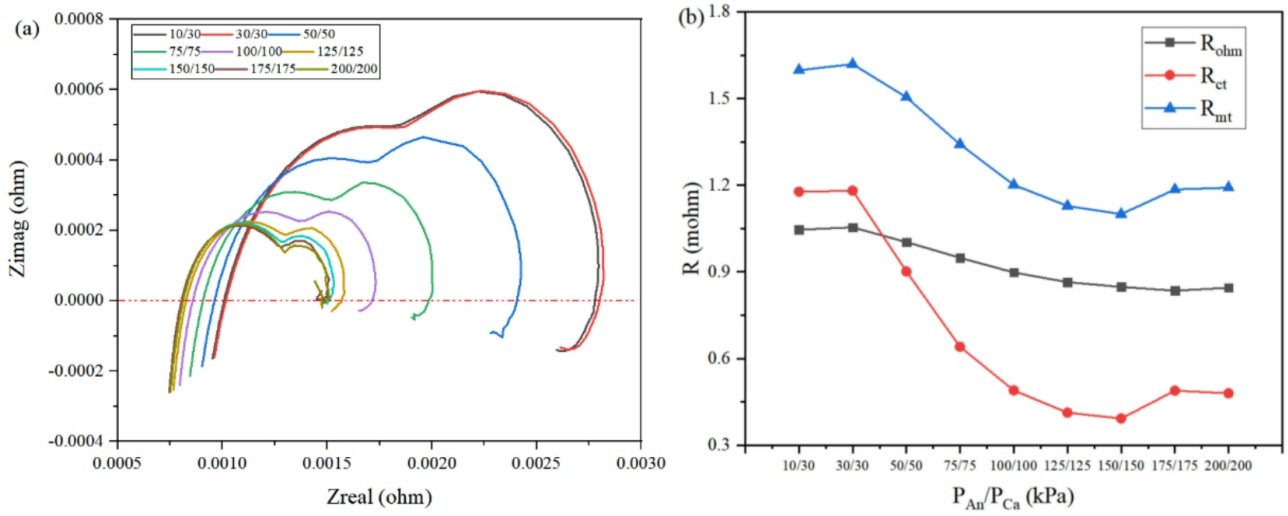


Figure 7

Impedance analysis: (a)Nyquist curve; (b) R_{ohm}, R_{ct} and R_{mt} under different gas pressures

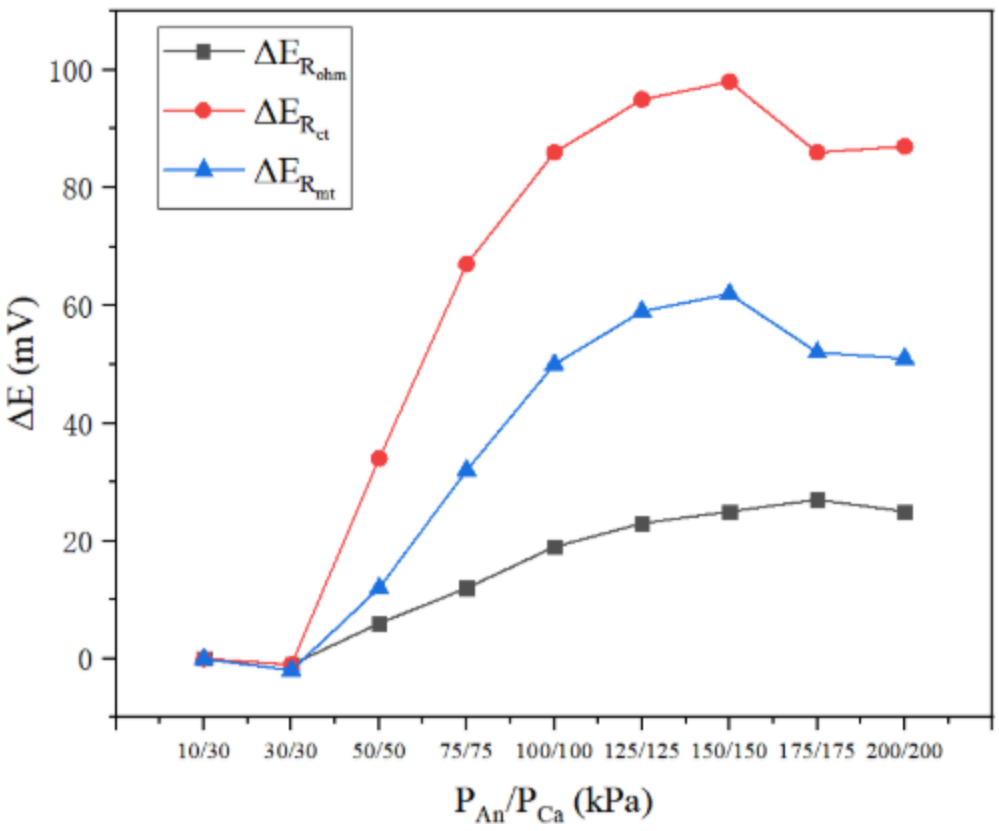


Figure 8

Voltage differences induced by each impedance under various gas pressures relative to 10/30kPa